Proceedings of the ASME 2014 Dynamic Systems and Control Conference
DSCC2014
October 22-24, 2014, San Antonio, TX, USA

DSCC2014-6352

TEMPERATURE ESTIMATION IN A BATTERY STRING UNDER FRUGAL SENSOR ALLOCATION

Xinfan Lin *
Anna G. Stefanopoulou
Jason B. Siegel

Department of Mechanical Engineering
University of Michigan
Ann Arbor, Michigan 48109
Email: xflin@umich.edu

Shankar Mohan
Department of Electrical Engineering
and Computer Science
University of Michigan
Ann Arbor, Michigan 48109

ABSTRACT

In electric vehicle applications, batteries are usually packed in modules to satisfy the energy and power demand. To facilitate the thermal management of a battery pack, a model-based observer could be designed to estimate the temperature distribution across the pack. Nevertheless, cost target in industry practice drives the number of temperature sensors in a pack to a number that is not sufficient to yield observability of all the temperature states. This paper focuses on formulating the observer design and sensor deployment strategy that could achieve the optimal observer performance under the frugal sensor allocation. The considered observer performance is the estimation errors induced by model and sensor uncertainty. The observer aims at minimizing the worst-case estimation errors under bounded model and sensor uncertainty.

INTRODUCTION

Thermal management is an important function of the battery management system (BMS) in electric vehicles (EVs). The electric current applied to the battery pack could be higher than 20 C-rate [1] for hybrid electric vehicles (FHEVs) operated in the Charge Sustaining (CS) mode. The aggressive battery usage may result in excessive temperature rise and a large temperature gradient across the cell, bringing challenges to thermal management. As far as safety is concerned, thermal runaway [1], which happens under extremely high temperature needs to be prevented. Furthermore, battery degradation is temperature dependent as the capacity and power fade is accelerated at high temperature [2–4]. Hence, the BMS needs to control battery temperature within designed ranges.

Model-based temperature estimation [5–7] is a key enabler for effective thermal management, which could provide detailed information about temperature distribution across the battery pack with limited number of temperature sensors. In [8], a thermal model for a one-dimensional battery string of cylindrical cells is constructed based on a single-cell thermal model, which captures the surface and core temperature of the cell, and cell-to-cell thermal interaction. Based on the thermal model and measurements of the surface temperatures of a few cells, an observer is designed to estimate all the temperature states in the string. These states include the surface and core temperature of all cells. It is highly desirable that the observer could i) significantly reduce the estimation errors under model uncertainty and ii) converge from erroneous initial estimation errors quickly. Since the thermal dynamics are stable, in an open-loop observer (without output feedback), the estimation error under model uncertainty will be bounded, and the errors caused by erroneous initial guess will die out eventually. However, because the thermal dynamics are slow, the eigenvalues of the model are close to the imaginary axis of the complex plane. The estimation errors could be large under model uncertainty, and the convergence from erroneous initial conditions would be slow. A closed-loop observer could guarantee i) and ii) if the model is fully observable. The numbers of temperature sensors needed for full observability have

*Address all correspondence to this author.

[1] C-rate refers to the magnitude of current, defined as the ratio between the current and the capacity of the battery in Ampere hour.

been determined from an observability analysis. For example, it is found that for a string with 10 cells, at least 4 sensor are needed to give full observability. However, the available sensors in a commercial battery pack is much less than the derived number, e.g. 16 for 288 cells in Chevy Volt and 42 for 288 cells in Toyota plug-in Prius. It may not be realistic to increase the number of sensors considering the cost and diagnostic requirement. Therefore, an interesting research problem is to find the best performance that can be achieved with the frugal sensor assignment which leaves the temperature states not completely observable.

In this paper, the observer design and sensor deployment problems for temperature estimation of battery strings are studied under unobservable conditions. The goal is to minimize the estimation errors under model and sensor uncertainty, which are assumed to be within a certain bound. The rest of the paper is organized as follows. First, the thermal model of a battery string is introduced. The estimation error of a closed-loop observer is then derived. Based on the derived estimation error, the observer design and sensor deployment problems are formulated as an optimization problem, which aim at minimizing the worst-case estimation error under all possible combinations of bounded model and sensor uncertainty. Finally, a drive-cycle simulation is used to show that the optimized observer could improve the overall estimation accuracy under dynamic current profile. Without loss of generality, a battery string with 10 cells and 1 temperature sensor will be considered as a design example.

THERMAL MODEL OF A ONE-DIMENSIONAL BATTERY STRING

A thermal model of a one-dimensional battery string has been constructed in [8], which is based on the single-cell thermal model studied in [9–11]. The schematic of a battery string and the thermal model is shown in Fig. 1.

The equivalent-circuit single-cell thermal model, as shown in the inset of Fig. 1, takes the form

$$\begin{aligned} C_c\frac{dT_c}{dt} &= Q+\frac{T_s-T_c}{R_c} \\ C_s\frac{dT_s}{dt} &= \frac{T_f-T_s}{R_u}-\frac{T_s-T_c}{R_c}, \end{aligned} \tag{1}$$

where the surface temperature T_s and the core temperature T_c are captured as the two states. The heat generation Q is modeled with a lumped internal resistance R_e [10] as

$$Q = I^2R_e, \tag{2}$$

where I is the current applied to the cell. It can also be computed based on a battery electrical model if available [12]. Heat exchange between the core and the surface is modeled by heat conduction over a thermal resistance, R_c, which is a lumped parameter aggregating the conduction and contact thermal resistance across the compact and inhomogeneous materials. A convection resistance R_u is modeled between the surface and the surrounding coolant to account for convective cooling. The value of R_u is a function of the coolant flow rate, and in some vehicle battery systems, the coolant flow rate is adjustable to control the battery temperature. Here, it is modeled as a constant as if the coolant flow rate is fixed to accommodate the maximum required cooling capacity. A model with the more complicated varying R_u has also been investigated in [11]. The rates of the temperature change of the surface and the core depend on their respective lumped heat capacity. The parameter C_c is the heat capacity of the jelly roll inside the cell, and C_s is related to the heat capacity of the battery casing.

$$\begin{aligned} C_c\frac{dT_{c,i}}{dt} &= I^2R_{e,i}+\frac{T_{s,i}-T_{c,i}}{R_c}, \\ C_s\frac{dT_{s,i}}{dt} &= \frac{T_{f,i}-T_{s,i}}{R_u}-\frac{T_{s,i}-T_{c,i}}{R_c}+Q_{cc,i}, \\ Q_{cc,i} &= \begin{cases} (T_{s,2}-T_{s,1})/R_{cc}, & i=1 \\ (T_{s,i-1}+T_{s,i+1}-2T_{s,i})/R_{cc}, & i=2,\cdots,n-1 \\ (T_{s,n-1}-T_{s,n})/R_{cc}, & i=n \end{cases} \\ T_{f,i} &= \begin{cases} T_{f,in}, & i=1 \\ T_{f,i-1}+\frac{T_{s,i-1}-T_{f,i-1}}{R_uC_f}, & i=2,\cdots,n \end{cases} \end{aligned} \tag{3}$$

A thermal model of a battery string is constructed by scaling up the single-cell thermal model and considering the cell to cell heat conduction [5] and heat balance of the flowing coolant [9, 13]. The string is considered as cells connected in series with tabs and arranged in a row configuration along the coolant flow path. The coolant flows through the space between cells from the inlet to the outlet, and picks up the heat dissipated from the cell surface through convection. For a string with n cells, the temperature evolution of the kth cell in a cluster can be modeled as in Eq.(3), where i is the index of the cell along the coolant flow direction. In the model, heat conduction between adjacent cells, Q_{cc}, is modeled as heat flow over a conduction resistance R_{cc}, driven by temperature difference between surfaces of the adjacent cells. It is noted here that R_{cc} is a lumped parameter, which includes heat conduction resistance of the tab and other possible connections between cells, such as the air gap. Coolant flow temperature entering the ith cell, $T_{f,i}$, is determined by heat balance of the flow around the previous cell, obtained by dividing the heat removed from the $i-1$th cell, $\frac{T_{s,i-1}-T_{f,i-1}}{R_u}$, by the heat capacity of the flow, C_f. The coolant temperature for the first cell is the inlet flow temperature $T_{f,in}$, which is regulated by the cooling system. Here, current I is same for all cells since the string is considered as in series connection. The individual cell internal resistance $R_{e,i}$ is not necessarily the same among all the cells, and the imbalance may be caused by factors such as manufacturing variability and degradation.

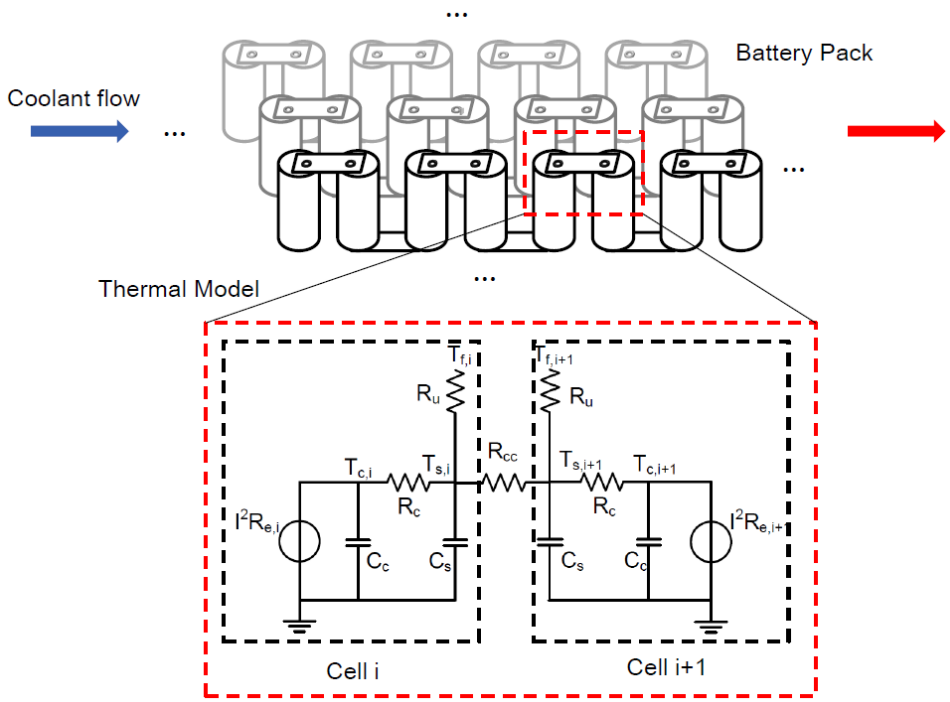

Figure 1. SCHEMATIC OF A ONE-DIMENSIONAL BATTERY STRING AND THE ASSUMED EQUIVALENT-CIRCUIT THERMAL MODEL.

The string thermal model in Eq. (3) can be written in the state space representation as

$$\begin{aligned} \dot{x} &= Ax + Bu, \quad x \in \mathbb{R}^{2n}, \quad u \in \mathbb{R}^2 \\ y &= Cx + \Delta y, \quad y, \Delta y \in \mathbb{R}^m \end{aligned} \tag{4}$$

where n is the number of cells and m is the number of sensors,

$$\begin{aligned} x &= \begin{bmatrix} T_{c,1} & T_{s,1} & T_{c,2} & T_{s,2} & \cdots & T_{c,n} & T_{s,n} \end{bmatrix}^T, \\ B &= \begin{bmatrix} \frac{R_{e,1}}{C_c} & 0 & \frac{R_{e,2}}{C_c} & 0 & \cdots & \frac{R_{e,n}}{C_c} & 0 \\ 0 & \frac{1}{R_u C_s} & 0 & \frac{1}{R_c C_s}\frac{R_u C_f - 1}{R_u C_f} & \cdots & 0 & \frac{1}{R_c C_s}\left(\frac{R_u C_f - 1}{R_u C_f}\right)^{n-1} \end{bmatrix}^T \\ u &= \begin{bmatrix} I^2 \\ T_{f,in} \end{bmatrix}. \end{aligned} \tag{5}$$

The matrix A is the state matrix shown in Eq.(6), y is the temperature state(s) measured by the sensor(s) whose location is specified in the C matrix, and Δy is the uncertainty in sensor measurement.

PROBLEM FORMULATION - OPTIMAL OBSERVER DESIGN FOR TEMPERATURE ESTIMATION

The objective in this paper is to design a model-based observer that could achieve optimal performance in temperature estimation under bounded uncertainty. The battery internal resistance typically varies from cell to cell due to factors such as degradation, manufacturing variability, and operating conditions [14, 15]. Since the observer can only use the nominal value $R_{e,0}$ for all the cells, there will be mismatch in battery resistance,

$$\begin{aligned} \Delta R_e &= \begin{bmatrix} \Delta R_{e,1} & 0 & \Delta R_{e,2} & 0 & \cdots & \Delta R_{e,n} & 0 \end{bmatrix}^T \\ &= \begin{bmatrix} R_{e,1} - R_{e,0} & 0 & R_{e,2} - R_{e,0} & 0 & \cdots & R_{e,n} - R_{e,0} & 0 \end{bmatrix}^T, \end{aligned} \tag{7}$$

which is the considered model uncertainty. The resistance uncertainty are usually within certain bounds to be specified later.

In this paper, the closed-loop observer for estimating the temperature states of the battery string takes the form

$$\begin{aligned} \dot{\hat{x}} &= A\hat{x} + B'u + L(y - \hat{y}) \\ \hat{y} &= C\hat{x}, \end{aligned} \tag{8}$$

where $\hat{x}$ and $\hat{y}$ denote the estimates of the states and outputs, and L is the observer gain. The input matrix is denoted as B' instead of B considering the uncertainty in internal resistance. The estimation error, e_x, is defined as the errors between x and $\hat{x}$,

$$e_x = x - \hat{x}. \tag{9}$$

The error dynamics can be derived by subtracting the observer

$$A = \begin{bmatrix}
\frac{-1}{R_cC_c} & \frac{1}{R_cC_f} & 0 & 0 & 0 & 0 & \cdots & 0 & 0 & 0 \\
\frac{1}{R_cC_s} & \frac{-1}{C_s}(\frac{1}{R_u}+\frac{1}{R_c}+\frac{1}{R_{cc}}) & 0 & \frac{1}{R_{cc}C_s} & 0 & 0 & \cdots & 0 & 0 & 0 \\
0 & 0 & \frac{-1}{R_cC_c} & \frac{1}{R_cC_f} & 0 & 0 & \cdots & 0 & 0 & 0 \\
0 & \frac{1}{C_s}(\frac{1}{{R_u}^2C_f}+\frac{1}{R_{cc}}) & \frac{1}{R_cC_s} & \frac{-1}{C_s}(\frac{1}{R_u}+\frac{1}{R_c}+\frac{2}{R_{cc}}) & 0 & \frac{1}{R_{cc}C_s} & \cdots & 0 & 0 & 0 \\
 & & & & & \ddots & & & & \\
0 & 0 & 0 & 0 & 0 & 0 & \cdots & 0 & -\frac{1}{R_cC_c} & \frac{1}{R_cC_f} \\
0 & \frac{1}{R_u^2C_fC_s}(1-\frac{1}{R_uC_f})^{n-2} & 0 & \frac{1}{R_u^2C_fC_s}(1-\frac{1}{R_uC_f})^{n-3} & 0 & 0 & \cdots & \frac{1}{C_s}(\frac{1}{{R_u}^2C_f}+\frac{1}{R_{cc}}) & \frac{1}{R_cC_s} & \frac{-1}{C_s}(\frac{1}{R_u}+\frac{1}{R_c}+\frac{1}{R_{cc}})
\end{bmatrix} \tag{6}$$

dynamics in Eq. (8) from the plant dynamics in Eq. (4), as

$$\dot{e}_x = (A-LC)e_x + \frac{\Delta R_e}{C_c}I^2 - L\Delta y, \quad e_x(t=0) = e_{x,0}. \tag{10}$$

The following section aims at finding the best observer performance that can be achieved given the thermal model and limited sensor allocation. The considered observer performance is the worst-case steady-state error induced by bounded model (resistance) and sensor uncertainty. It will be shown later that the observer could also reduce the estimation errors under dynamic current input.

Minimization of Worst-Case Steady-State Estimation Error under Model Uncertainty

The steady-state error under a constant current (or symmetric charging-discharging current pulse train) can be obtained based on Eq. (10) as

$$e_{x,\infty} = -(A-LC)^{-1}(\frac{\Delta R_e}{C_c}I^2 - L\Delta y). \tag{11}$$

The error $e_{x,\infty}$ is a $2n \times 1$ vector, consisting of the steady-state error in each of the temperature state. Here, the performance of the observer is evaluated based on the largest error in all the states, which is represented by the infinity norm of $e_{x,\infty}$,

$$\|e_{x,\infty}\|_\infty = \|(A-LC)^{-1}(\frac{\Delta R_e}{C_c}I^2 - L\Delta y)\|_\infty. \tag{12}$$

Other norms, such as the 2-norm, can also be chosen as the criterion. In Eq.(12), the resistance uncertainty, ΔR_e, and sensor uncertainty, Δy, are usually within certain bounds. It is assumed here that each $\Delta R_{e,i}$ is bounded within $\pm 10\%$ of the nominal value,

$$-0.1R_{e,0} \le \Delta R_{e,i} \le 0.1R_{e,0}, \quad \forall i = 1,2,\cdots,n \tag{13}$$

and the uncertainty of each temperature sensor, Δy_j, is bounded within $\pm 0.5^oC$ (typical of the T-type thermocouple),

$$-0.5^oC \le \Delta y_j \le 0.5^oC, \quad \forall j = 1,2,\cdots,m. \tag{14}$$

Most likely, assigning a sensor on the cell with the largest resistance uncertainty will help reduce the estimation errors. However, since no priori knowledge on the location of the cell with the largest uncertainty is available, we assume that each $\Delta R_{e,i}$ follows uniform distribution within the specified bounds.

Based on the infinity norm of the estimation error obtained in Eq.(12), the observer design and sensor deployment problems can be formulated as optimization problems at the following three different level.

i) Performance Evaluation: the performance of an observer (given sensor location specified in C and observer gain L) is defined as the worst-case steady-state error under all ΔR_e and Δy,

$$\begin{aligned}
&\max_{\Delta R_e, \Delta y} \|(A-LC)^{-1}(\frac{\Delta R_e}{C_c}I^2 - L\Delta y)\|_\infty \\
&\Delta R_e = \begin{bmatrix}\Delta R_{e,1} & 0 & \Delta R_{e,2} & 0 & \cdots & \Delta R_{e,n} & 0\end{bmatrix}^T, \\
&\Delta y = \begin{bmatrix}\Delta y_1 & \Delta y_2 & \cdots & \Delta y_m\end{bmatrix}^T, \\
&s.t. -0.1R_{e,0} \le \Delta R_{e,i} \le 0.1R_{e,0}, \quad i = 1,2,\cdots,n \\
&\quad -0.5^oC \le \Delta y_j \le 0.5^oC, \quad j = 1,2,\cdots,m.
\end{aligned} \tag{15}$$

ii) Observer Design: if the sensor location C is fixed but the observer gain L remains to be designed, an optimal observer could look at minimizing the worst-case error,

$$\min_L \max_{\Delta R_e, \Delta y} \|(A-LC)^{-1}(\frac{\Delta R_e}{C_c}I^2 - L\Delta y)\|_\infty, \tag{16}$$

subject to the same constraints in Eq.(15).

iii) Sensor Deployment: if the sensor location C could also be chosen, the sensor deployment problem will be

$$\min_{C}\min_{L}\max_{\Delta R_e,\Delta y}\|(A-LC)^{-1}(\frac{\Delta R_e}{C_c}I^2-L\Delta y)\|_\infty, \quad \text{C s.t. permissible sensor locations.} \tag{17}$$

If a battery string of 10 cells is considered and one sensor is available, the total number of permissible C is 10, which measures the surface temperature of each cell respectively. For example, when the one sensor is allocated at Cell 1, the C matrix will be $\begin{bmatrix}0 & 1 & 0 & 0 & \cdots & 0 & 0\end{bmatrix}$. The optimal C^* needs to be found among all 10 permissible C's.

The first step is to find the worst-case error by solving the maximization problem in Eq.(15) when C and L are given. It is noted that the $2n\times 1$ vector $(A-LC)^{-1}(\Delta R_e I^2-L\Delta y)$ can be viewed as $2n$ linear and thus convex functions with respect to ΔR_e and Δy. The infinity norm of $(A-LC)^{-1}(\Delta R_e I^2-L\Delta y)$ will still be convex to ΔR_e and Δy, since the maximum of multiple convex functions is still a convex function [16]. As ΔR_e and Δy are bounded by box constraints shown in Eq.(15), the permissible ΔR_e and Δy form a compact convex set. According to the the maximum principle [17], the maximum of the convex cost function in Eq.(15) is attained on the boundary (or vertices) of the convex compact set formed by ΔR_e and Δy. The boundary is defined by the combinations of ΔR_e and Δy, whose elements, $\Delta R_{e,i}$ and Δy_i, take either the upper bound or the lower bound,

$$\begin{aligned}\Delta R_{e,i} &= 0.1R_{e,0} \text{ or } -0.1R_{e,0}, \quad \forall i=1,\cdots,n\\ \Delta y_i &= 0.5^oC \text{ or } -0.5^oC, \quad \forall i=1,\cdots,m.\end{aligned} \tag{18}$$

The maximization problem in Eq.(15) is hence transformed to

$$\begin{aligned}&\max_{\Delta R_e,\Delta y}\|(A-LC)^{-1}(\frac{\Delta R_e}{C_c}I^2-L\Delta y)\|_\infty\\ &\Delta R_e=\begin{bmatrix}\Delta R_{e,1} & 0 & \Delta R_{e,2} & 0 & \cdots & \Delta R_{e,n} & 0\end{bmatrix}^T\\ &\Delta y=\begin{bmatrix}\Delta y_1 & \Delta y_2 & \cdots & \Delta y_m\end{bmatrix}^T,\\ &s.t.\quad \Delta R_{e,i}\in\{0.1R_{e,0},-0.1R_{e,0}\},\quad \Delta y_i\in\{0.5^oC,-0.5^oC\}.\end{aligned} \tag{19}$$

For the case of 1 sensor in 10 cells, there are a total of 10 $\Delta R_{e,i}$ that could take either $0.1R_{e,0}$ or $-0.1R_{e,0}$, and 1 Δy_i that could take either 0.5^oC or -0.5^oC. Hence the total number of vertices is $2^{10+1}=2048$. The worst-case error can be found by evaluating the cost function at these 2048 vertices and choosing the maximum.

The next step is to design the observer gain L to minimize the worst-case error by solving Eq.(16). The traditional methods for observer design, such as Kalman filtering and pole placement, are not suitable for this problem. The Kalman filter, which seeks the optimal estimation under Gaussian process and measurement noises, will not necessarily be the optimal observer here under bounded constant model uncertainty. For pole placement, it is not clear how to find the optimal pole locations to minimize the worst-case estimation error. Therefore, several optimization methods have been attempted for the optimal observer design, which include applying a) Matlab command `fmincon` and b) Matlab command `fminimax`. The application of a) is straightforward. For b), the built-in Matlab command `fminimax` is designed to minimize the maximum of a set of functions, which share a common variable. Here, the function set consists of the cost function Eq.(12) evaluated at each vertex in Eq.(18), and the common variable is the observer gain L. It needs to be pointed out that the above problem is not convex optimization, as the cost functions are non-convex. Consequently, the optimization results may fall into local minimum. In order to reduce the likelihood of encountering local minimum, the two methods have been attempted under different initial guesses during the optimization procedures. For the case to be demonstrated, the same minimum worst-case errors $\|e_{x,\infty}\|_\infty^*$ have been obtained. The optimized observer gains L^* are not exactly the same though, probably because the thermal model is not completely observable. Since the observer gain L will not have much effect on the unobservable subspace, some entries of L, which mainly associated with the unobservable subspace, could be non-unique when achieving the minimum worst-case error. The obtained observer gains have also been checked to satisfy the stability condition as $A-LC$ is Hurwitz.

Finally, for the sensor deployment problem in Eq.(17), the optimal sensor location (C) can be determined by solving Eq.(16) for all permissible sensor locations and choosing the one with the minimum error.

The outlined optimization procedures have been applied to a cell string with 10 cells, and the cases when only 1 temperature sensor is available are considered. The optimized worst-case estimation errors in steady state under 10 C constant current for each sensor location are shown in Fig. 2. The dashed line shows the worst-case steady-state estimation error under open loop, and the solid line shows the errors under the optimized observer for different sensor locations. It can be seen that the optimal sensor location is at Cell 8, and the minimal worst-case estimation error is 3.15^oC, reduced from 4.26^oC under open loop. As seen in the figure, the optimized estimation errors are large when the sensor is placed at the surface of the first few cells, and decrease as the sensor is moved to the middle section of the string. After achieving the minimum at Cell 8, the estimation error starts to increase again towards the end. The cases of ΔR_e^* that yield the worst-case errors under open loop and some sensor locations are demonstrated in Fig. 3. It is shown that ΔR_e^*, which is the combination of the cell resistance uncertainty that corresponds to the worst-case estimation error, is different for different sensor locations. It is also interesting to investigate the distribution of the steady-state estimation error at all the vertices specified in Eq.(18). As an example, the error distribution when the sensor

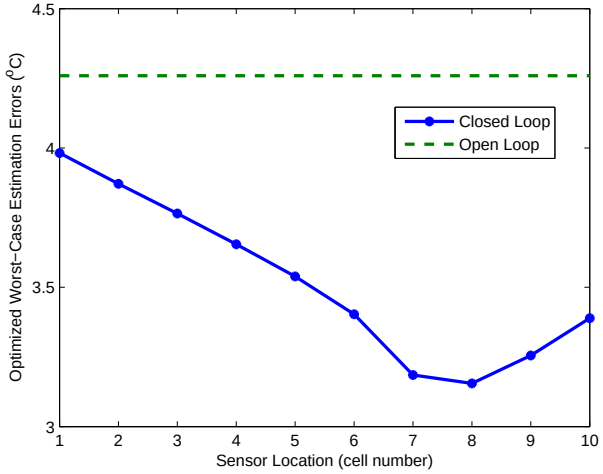

Figure 2. Optimized worst-case estimation errors in steady state at each sensor location when 1 sensor is available for 10 cells (under $20\ C$ constant current).

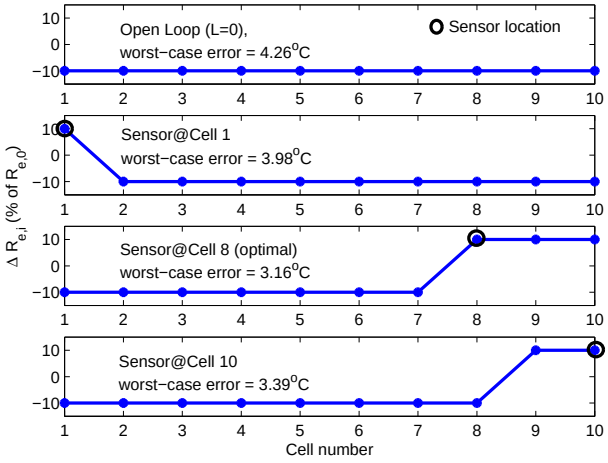

Figure 3. Cases of ΔR_e distribution across the cells giving the worst-case estimation errors under different sensor locations.

is placed at Cell 8 is shown by the histogram in Fig. 4. The x-axis denotes the values of the infinity norm of the steady-state errors, and the y-axis shows the occurrence of the error values among the vertices as a percentage of the total number of vertices. The characteristics of the error distribution, including the maximum (worst-case), mean and median, are also denoted in the figure for both open loop and the optimized observer. It is noted that while the optimized observer reduces the worst-case error by 1.1^oC as compared to that in open loop, the mean and the median of the errors at all the vertices do not see a significant improvement. The reason might be attributed to the fact that the

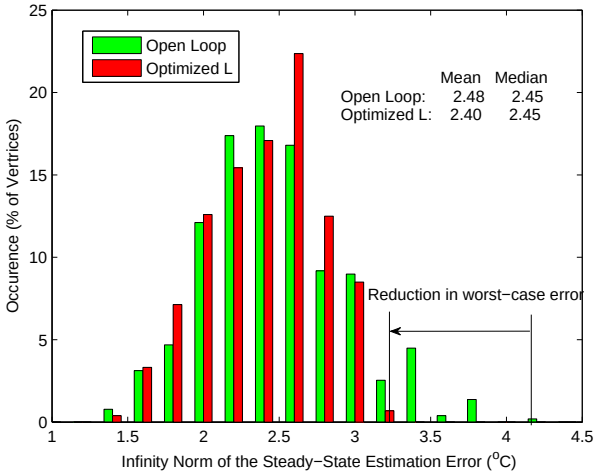

Figure 4. Distribution of the steady-state error norm at all vertices under open loop and optimized observer (sensor located at cell 8). Vertices: the combinations of ΔR_e, each element of which takes either the upper bound $0.1R_{e,0}$ or the lower bound $-0.1R_{e,0}$, as specified in Eq.(18).

battery string model is unobservable when only one surface temperature is measured. The moderate reduction in worst-case error and insignificant improvement in error mean and median may reflect the fundamental limitation imposed by the unobservability, but the detailed mechanism remains to be investigated.

SIMULATION UNDER A DRIVE-CYCLE

In this section, the performance of the designed observer is evaluated under drive-cycle simulation. It is shown that the observer, though designed primarily to minimize the steady-state estimation error, could also improve the estimation accuracy under dynamic current profile. Besides model uncertainty, the temperature estimation may also be affected by errors in initial guesses. This issue is of particular interest for the following reasons. First, at every start-up, initial temperature gradient could exist in a battery pack caused by factors such as external conditions and insufficient relaxation from previous operation [8, 18]. Due to the scarcity of the temperature sensor, the temperature gradient would turn into error in initial temperature estimation. Second, under open loop, although the initial errors would eventually die out since the thermal system is stable, the convergence would be seriously delayed by the slow battery thermal dynamics [8]. This aspect is also considered in the drive-cycle simulation.

The considered drive cycle is plotted in Fig. 5, where the top plot shows the current profile in C-rate. The evolution of the highest temperature, which is the core temperature of Cell 10 $T_{c,10}$, and the lowest temperature, namely the surface temperature of Cell1 $T_{s,1}$, are demonstrated in the bottom plot to show the temperature gradient across the battery string. The current

profile consists of three parts, a first sub-cycle, a 5 mins rest, and a second sub-cycle. Because the rest between the two sub-cycles are very short, the cells would not reach thermal equilibrium at the end of the rest, and temperature gradient exists across cells at the start of the second sub-cycle. Since only one temperature sensor is available, the reading of the sensor will be used to initialize all the temperature estimation, leading to initial errors in most states. The performance of the open-loop and the optimized observer during the second sub-cycle is plotted in Fig. 6, which shows the maximum estimation error among all the states, $\max|e_x|$, at each time instant. The assumed resistance uncertainty ΔR_e is the first case shown in Fig. 3, and the optimized observer is the one with sensor at cell 8. It can be seen that the optimized observer could not only reduce the estimation errors when the temperature states enter the "semi steady-state" after around t = 4000 s, but also accelerate the convergence from the initial estimation error. The performance of the observers can be evaluated based on the normalized L_2-norm of the maximum estimation error,

$$\|e_{x,max}(t)\|_{L_2} = \Big(\int_0^T (max|e_x(t)|)^2 dt\Big)^{\frac{1}{2}}/T, \qquad (20)$$

where T is the duration of the cycle. The distribution of $\|e_{x,max}(t)\|_{L_2}$ at all the vertices specified in Eq.(18) is shown in the histogram in Fig. 7. The x-axis denotes the values of the L_2-norm of the maximum estimation error, and the y-axis shows the occurrence of the error values among the vertices as a percentage of the total number of vertices. The characteristics of the error distribution, including the maximum (worst-case), mean and median, are also denoted in the figure for both open loop and the optimized observer. Improvement of the estimation accuracy similar to that in steady-state shown in Fig. 4 is observed.

CONCLUSION

In this paper, temperature estimation in battery string is studied under frugal sensor allocation. Optimal observers are designed to minimize the estimation error under model/sensor uncertainty. The estimation problem is formulated as optimization problems in three different levels. The first level involves determining the worst-case error under bounded uncertainty or initial errors, which is defined as the performance of the observer. In the second level, the observer gain is designed to minimize the worst-case errors. The third level addresses the sensor deployment problem by selecting the sensor location that allows the best observer performance. With the designed observer and sensor location, it is guaranteed that the steady-state estimation errors for all the temperature states will be within the specified limit as long as the assumed bounds on model uncertainty and initial conditions hold. As shown in drive-cycle simulation, the observer could also accelerate the convergence of the estimation from erroneous initial errors and improve the overall estimation accuracy under dynamic current profile. A battery string model

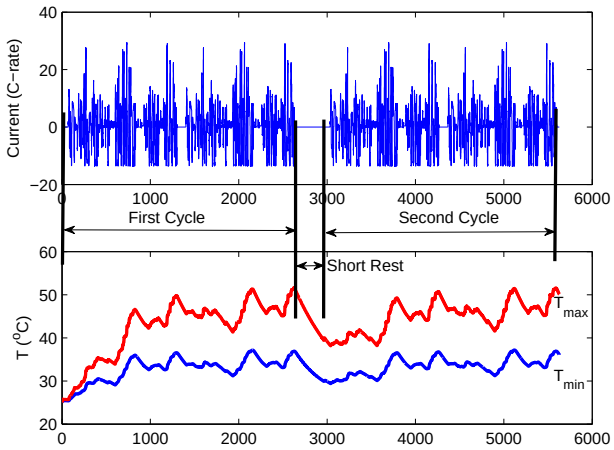

Figure 5. Drive-cycle Simulation (top plot: current in C-rate; bottom plot: evolution of highest temperature $T_{c,10}$ and lowest temperature $T_{s,1}$.

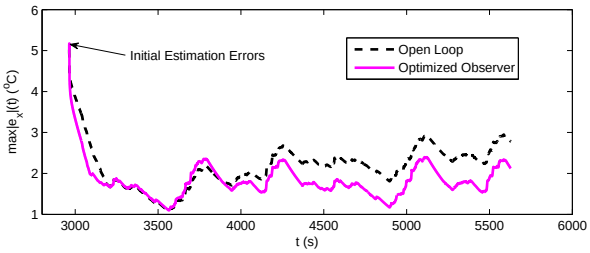

Figure 6. Evolution of the maximum estimation error among all states over time.

with 10 cells and 1 sensor is used as an example to illustrate the introduced methodology. The presented worst-case temperature estimation errors may not be considered as critical by some standards (even for the open loop estimation), which might justify the frugal sensor allocation that is being applied in the industry practice. It may also be due to the specific parameters and configuration of the battery string that is considered. The methodology developed here can be applied to other battery packs, whose parameters and configuration may induce more significant estimation errors in temperature estimation.

ACKNOWLEDGMENT

REFERENCES

[1] Bandhauer, T. M., Garimella, S., and Fuller, T. F., 2011. "A critical review of thermal issues in lithium-ion batteries". *Journal of The Electrochemical Society,* **158**, pp. 1–25.

[2] Thomas, E., Case, H., Doughty, D., Jungst, R., Nagasubramanian, G., and Roth, E., 2003. "Accelerated power

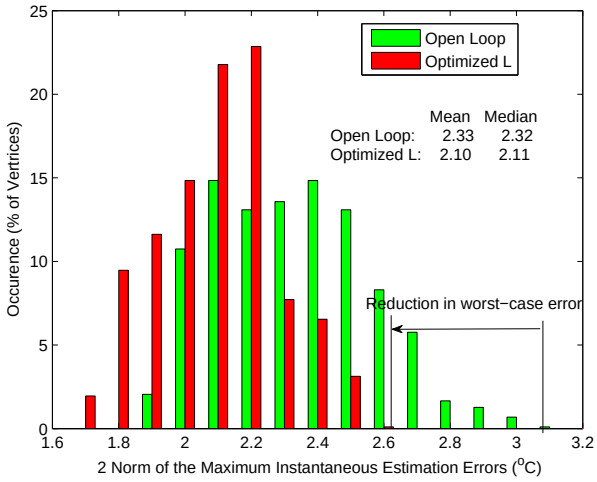

Figure 7. Distribution of the L_2-norm of maximum instantaneous estimation errors over the cycle at all vertices under open loop and optimized observer (sensor located at cell 8).

degradation of li-ion cells". *Journal of Power Sources,* **124**, pp. 254–260.

[3] Amine, K., Liu, J., and Belharouak, I., 2005. "High-temperature storage and cycling of c-lifepo4/graphite li-ion cells". *Electrochemistry Communications,* **7**, pp. 669–673.

[4] Liu, P., Wang, J., Hicks-Garner, J., Sherman, E., Soukiazian, S., Verbrugge, M., Tataria, H., Musser, J., and Finamore, P., 2010. "Aging mechanisms of lifepo4 batteries deduced by electrochemical and structural analyses". *J. Electrochem. Soc.,* **157**, pp. 499–507.

[5] Smith, K., Kim, G.-H., Darcy, E., and Pesaran, A., 2010. "Thermal/electrical modeling for abuse-tolerant design of lithium ion modules". *International Journal of Energy Research,* **34**, p. 204C215.

[6] Forgez, C., Do, D., Friedrich, G., Morcrette, M., and Delacourt, C., 2010. "Thermal modeling of a cylindrical lifepo4/graphite lithium-ion battery". *Journal of Power Sources,* **195**(9), May, pp. 2961–2968.

[7] Debert, M., Colin, G., Bloch, G., and Chamaillard, Y., 2013. "An observer looks at the cell temperature in automotive battery packs". *Control Engineering Practice,* **21**, pp. 1035–1042.

[8] Lin, X., Fu, H., Perez, H. E., Siegel, J. B., Stefanopoulou, A. G., Ding, Y., and Castanier, M. P., 2013. "Parameterization and observability analysis of scalable battery clusters for onboard thermal management". *Oil & Gas Science and Technology ł Rev. IFP Energies nouvelles, France,* **68**, pp. 165–178.

[9] Park, C., and Jaura, A., 2003. "Dynamic thermal model of li-ion battery for predictive behavior in hybrid and fuel cell vehicles". In SAE 2003-01-2286.

[10] Lin, X., Perez, H., Siegel, J., Stefanopoulou, A., Li, Y., Anderson, R. D., Ding, Y., and Castanier, M., 2013. "Online parameterization of lumped thermal dynamics in cylindrical lithium ion batteries for core temperature estimation and health monitoring". *IEEE Transactions on Control Systems Technology,* **21**, pp. 1745–1755.

[11] Lin, X., Perez, H., Siegel, J., Stefanopoulou, A., Li, Y., and Anderson, R. D., 2012. "Quadruple adaptive observer of li-ion core temperature in cylindrical cells and their health monitoring". In American Control Conference.

[12] Lin, X., Perez, H. E., Mohan, S., Siegel, J. B., Stefanopoulou, A. G., Ding, Y., and Castanier, M. P., 2014. "A lumped-parameter electro-thermal model for cylindrical batteries". *Journal of Power Sources,* **257**, pp. 1–11.

[13] Mahamud, R., and Park, C., 2011. "Reciprocating airflow for li-ion battery thermal management to improve temperature uniformity". *Journal of Power Sources,* **196**, pp. 5685–5696.

[14] Dubarry, M., Vuillaume, N., and Liaw, B. Y., 2009. "From single cell model to battery pack simulation for li-ion batteries". *Journal of Power Sources,* **186**, pp. 500–507.

[15] Dubarry, M., Vuillaume, N., and Liaw, B. Y., 2010. "Origins and accommodation of cell variations in li-ion battery pack modeling". *International Journal of Energy Research,* **34**, pp. 216–231.

[16] Boyd, S., and Vandenberghe, L., 2004. *Convex Optimization*. Cambridge University Press.

[17] Rockafellar, R. T., 1997. *Convex Analysis*. Princeton University Press.

[18] Pesaran, A. A., 2002. "Battery thermal models for hybrid vehicle simulations". *Journal of Power Sources,* **110**, pp. 377–382.